Landslides (2019) 16:1645–1661
DOI 10.1007/s10346-019-01196-6
Received: 18 December 2018
Accepted: 2 May 2019
Published online: 5 June 2019

Chi Liu · Xiaoli Liu · Xiaochu Peng · Enzhi Wang · Sijing Wang

Application of 3D-DDA integrated with unmanned aerial vehicle–laser scanner (UAV-LS) photogrammetry for stability analysis of a blocky rock mass slope

Abstract In stability analysis of discontinuity-controlled slopes, the rationality of results is related to the accuracy of three-dimensional (3D) slope morphology and the reliability of the discontinuity survey. With the advent of remote sensing technologies for engineering geological surveys and slope stability analyses, step-change increases have been made in the quality of data available and geometrical characterization of rock slopes. Although these techniques are frequently employed in the characterization of slope geometry and joint surfaces at present, limited research has been undertaken to effectively process the derived data and improve the quality in the reconstruction of slope geometry imported into 3D discontinuous numerical models. In this paper, an integrated system coupling 3D-DDA and UAV-LS photogrammetry is presented as a tool to evaluate the stability of a blocky rock mass slope. The system includes a UAV-LS module, a modeling module, a block-generation module, and a 3D-DDA calculation module. In the UAV-LS module, the use of UAV-LS system integrated with field mapping and site observations allows the acquisition of detailed outputs (point clouds) on both the slope and discontinuity geometry. An effective combination of commercial software Geomagic and Hyperworks is used in the modeling module to process oceans of 3D point cloud data and construct complex 3D geometrical models based on reverse engineering. In the block-generation module, the three-dimensional discontinuous deformation analysis (3D-DDA) method is then carried out in order to simulate the movement of potentially unstable blocks, within which an independent block-cutting algorithm is used to generate the blocks with arbitrary shapes and the finite structural planes similar to the real cases. The 3D-DDA calculation module uses 3D-DDA calculation algorithm to derive the simulation results. The capability of the proposed system for stability analysis of a jointed slope is demonstrated by a practical example.

Keywords Stability analysis · Remote sensing · 3D discontinuous numerical models · System · 3D-DDA · UAV-LS photogrammetry · Reverse engineering

Introduction

Rockfalls generated by rocks that detach from parent rocks and roll downhill are a prevalent and frequent type of the instability of steep slopes. For structural design and disaster prevention, many numerical methods have been developed to simulate and analyze the stability of slopes. In the field of geotechnical engineering, continuum-based methods (Cervera et al. 2017; Chen et al. 2013; Wu and Li 2015) and discontinuum-based (Fakhimi et al. 2002; Hazzard and Young 2000; Kazerani et al. 2012; Shi and Goodman 1984) methods are two main numerical tools. Finite element method (FEM) and finite difference method (FDM) are typical continuum-based methods, which have already been successfully applied in engineering problems where the rock mass does not stand large deformation. Therefore, slopes dominated by discontinuities (joints) usually have complicated geometry and mechanical properties are difficult to be simulated based on continuum-based models. To reasonably assess the stability of rock mass, discontinuous numerical modeling is required.

Discontinuous deformation analysis termed as DDA (Shi and Goodman 1984, 1989) is a powerful discontinuum-based numerical method in simulation of large displacement and large deformation problems controlled by discontinuities. This code employs implicit time integration scheme, which can ensure the accuracy and stability of numerical calculation under the premise of a larger time step. Regarding the solution scheme, the governing equation in DDA is established and solved directly according to the principle of minimization of the total potential energy of the block system, which ensures strict equilibrium conditions (Shi 2009). The simplex integration method is used in DDA to ensure the accuracy of calculation results when blocks with arbitrary shapes are established (Fan et al. 2018; Keneti and Jafari 2008; Wu 2010a). In the contact mechanics, the contact between blocks, usually called penalty method, is considered to be rigid and no interpenetration or no tension is required to ensure that the mathematical and numerical description of mechanical behavior is consistent with the movement of blocks. Many great improvements and extensions have been made to the original codes over the past three decades in many aspects such as contact mechanics algorithm (Beyabanaki et al. 2008; Jiang and Yeung 2004), convergence criteria (Jiang et al. 2013), crack simulation (Cai et al. 2013; He and Ma 2010; Zhang and Wong 2013), and coupling algorithm with other methods such as DDA-SPH (Wang et al. 2016) and FEM-DDA (Kaidi et al. 2012). Besides, the application of DDA is becoming more and more extensive including the simulation of the movement of landslides under the premise of seismic loadings (Wu 2010b; Wu and Chen 2011; Wu et al. 2009; Zhang et al. 2013), the analysis of rockfalls from slope surface (Chen 2003; Chen et al. 2013; Ma et al. 2011), and stability analysis of tunnels (Wu et al. 2018). In many practical examples, 2D-DDA is used to analyze problems. However, 3D topography and 3D geometry of the jointed rock mass are important for stability, thus 3D-DDA should be used.

One of the fundamental difficulties in implementing 3D-DDA method on slopes controlled by discontinuities is establishing 3D discontinuous models. In stability analysis of discontinuity-controlled slopes, the rationality of results is related to a large degree by the veracity of three-dimensional (3D) slope topology and the reliability of the discontinuity survey. In real cases, geological bodies usually have complex geometrical characterization, which is difficult for surveyors to employ the traditional means of field investigations, field mapping, and geological compasses for

Table 1 Technical parameters of the UAV used in the study

Key parameters	Value
Weight (kg)	9.5
Take-off-weight (kg)	15.5
Wheel base (mm)	1133
Maximum flight time (min)	32
Maximum flight speed (m/s)	18
Maximum flight height (m)	2500

data collection. For large-scale geological bodies like rock slopes, traditional geological survey is time-consuming and the results are sometimes subjective and arbitrary, which can lead engineers to misjudge the stability of geological bodies. Over the last two decades, the advent of remote sensing technologies for engineering geological surveys and slope stability analyses has led to dramatic improvement in the quality in data available and geometrical characterization of rock slopes. The most common techniques are digital photogrammetry (DP) and 3D laser scanning (LS) applied in the research of natural and engineered slopes that have been discussed by many researchers (Coggan et al. 2007; Francioni et al. 2015; Francioni et al. 2014; Ghirotti and Genevois 2007; Lato et al. 2009; Riquelme et al. 2017; Salvini et al. 2013; Spreafico et al. 2016; Sturzenegger and Stead 2009a, b). These technologies allow for the acquisition and document of very detailed information like millions of rock surface point locations in space on the slope geometry, which can be much more extensive and accurate than what is obtained by site observations and hand-mapping in traditional geological data collection. The data collected by DP and LS can provide very relevant input information for stability analysis of rockmass slope, especially when considering a large number of software now available for both conventional and numerical methods of stability analysis (Stead and Wolter 2015).

As for remote sensing platforms, ground-based platforms and airborne platforms are two significant types. The instruments of ground-based remote sensing platforms such as hand-held devices, tripods, and vehicles are commonly used in engineering geology. These platforms have been successfully applied by several authors in the analysis of rockmass slopes (Bonilla-Sierra et al. 2015; Haneberg et al. 2006; Havaej et al. 2016). Although ground-based instruments are cost-effective and easy to use, significant limitations related to the slope elevation are inevitable. Despite the high quality of point clouds and photographs, the observation point at the nadir is sub-optimal in the case of artificial and natural rockmass slopes characterized by extremely steep or even vertical slope surfaces. When conducting a survey at the bottom of a steep and high slope, occlusion is an important factor that can seriously compromise the veracity of the final model (Francioni et al. 2014; Lato et al. 2009). As for airborne platforms, satellite/airplane (Clayton et al. 2017; Donati et al. 2017; Mantovani et al. 2016; Wolter et al. 2016), aerostatic balloon (Take et al. 2007; Firpo et al. 2011; Francioni et al. 2014), helicopter (Salvini et al. 2013; Salvini et al. 2011), and UAV (Francioni et al. 2015; Niethammer et al. 2012; Westin 2017) are the most commonly used instruments currently available, with which the observation point can be changed and the occlusion problem highlighted for the ground-based platforms can be reduced significantly even if in the case of steep or even vertical inaccessible slopes. Recently, notable progress has been made in small-scale techniques that enable the UAV to be an alternative remote sensing platform offering extremely high-resolution captured data with high quality at a significantly lower survey cost. High-resolution point cloud data can be easily collected by a UAV equipped with a large number of navigation sensors combined with on-board LS sensors. High-quality aerial photos can also be obtained using UAV photogrammetry. The processing of the data available using remote sensing techniques and the digital aerial photos is inevitable (Riquelme et al. 2019). Besides, the accuracy of the final model is influenced to a large degree by the time cost and refinement of the processing of massive data.

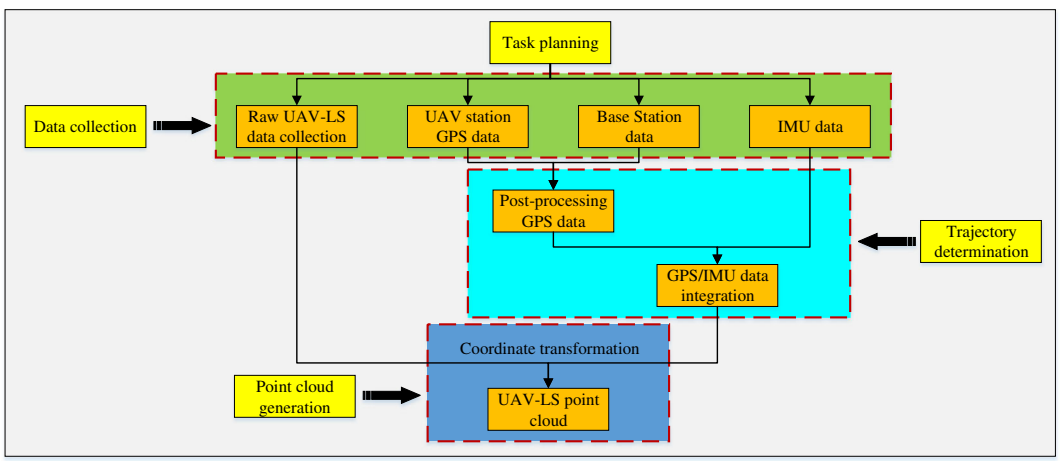

Fig. 1 Workflow of the generation of UAV-LS point clouds

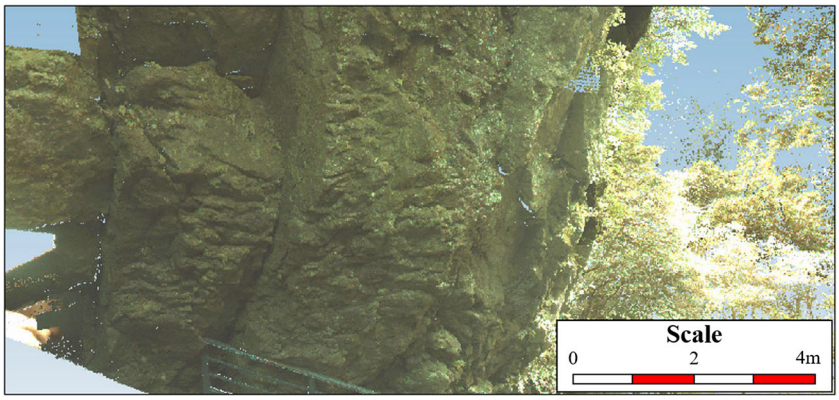

Fig. 2 UAV-LS photogrammetry

It should be noted that wherever possible, remote sensing approaches should be supplemented with photographic site observations and field mapping. The structural planes of rockmass slope can be determined by both conventional and remote sensing methods. For many practical applications, rock mass usually has complex arbitrary geometries mainly due to discontinuities. Therefore, it is very important to have a block-cutting algorithm to cut the rock mass into a large quantity of blocks directly from 3D topography based on 3D structural planes.

The purpose of this paper is to demonstrate a system integrating unmanned aerial vehicle–laser scanning (UAV-LS) photogrammetry with 3D-DDA method for modeling and stability analysis of a blocky rock mass slope. This system contains four modules: the UAV-LS module, the modeling module, the block-generation module, and the 3D-DDA calculation module. In the UAV-LS module, the use of UAV-LS system combined with field mapping and site observations allows the collection of detailed outputs (point clouds) on both the slope and discontinuity geometry for the analysis of the potential rock slope instability mechanisms. In the modeling module, an effective combination of commercial software Geomagic and Hyperworks is used to process huge volumes of point cloud data and construct complex 3D geological models. In the block-generation module, the three-dimensional discontinuous deformation analysis (3D-DDA) method, an appropriate numerical method to solve large deformation and large displacement problems controlled by discontinuities, is carried out in order to simulate the movement of potentially unstable blocks, within which an standalone block-cutting algorithm is used to generate the blocks with arbitrary shapes and the finite structural planes similar to the real cases. In the 3D-DDA calculation module, the simulation results are derived using 3D-DDA calculation algorithm. A practical application in which a slope with jointed rock mass is simulated using this system.

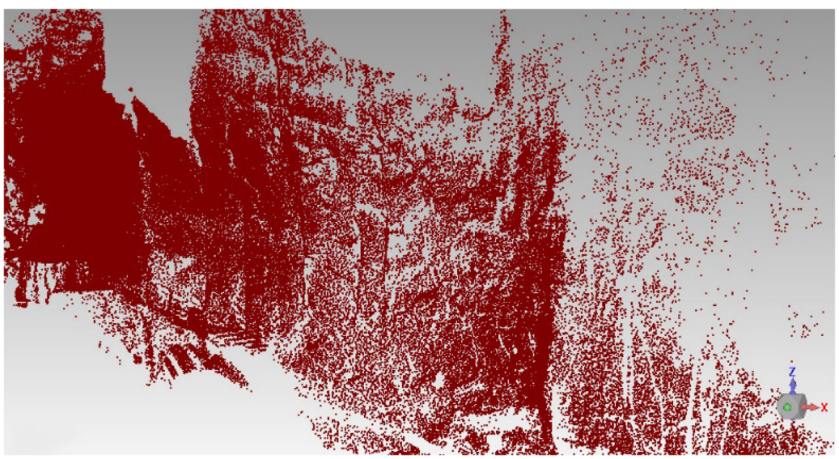

Fig. 3 3D point clouds

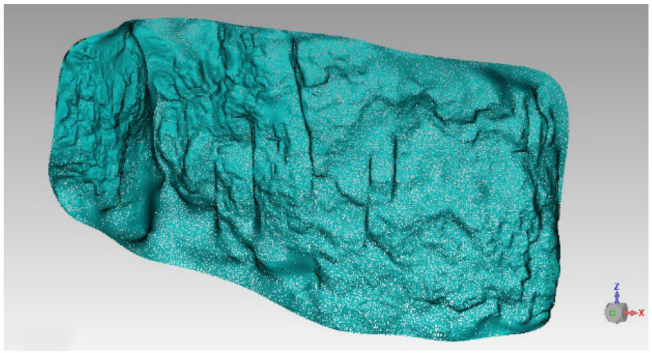

(a) Point cloud filtering

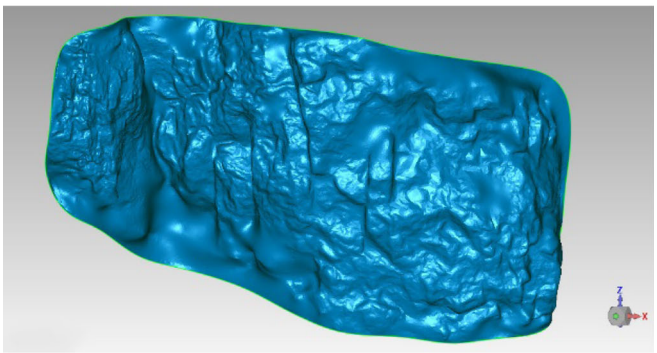

(b) Point cloud encapsulation

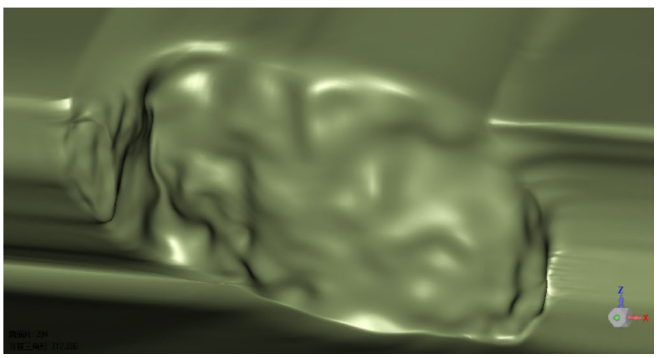

(c) NURBS model

Fig. 4 Point cloud processing

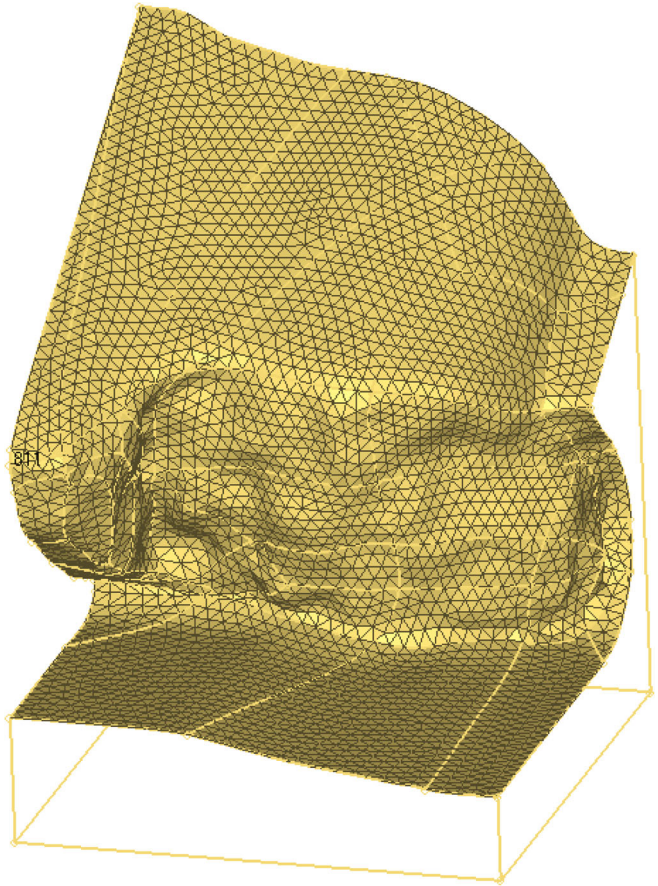

Fig. 5 Mesh generation

Devices and methodology

UAV-LS platform

The UAV platform used in this study in the UAV-LS module includes a ground control system and a multi-rotor UAV (DJI M600 PRO) with the Velodyne VLP-16 laser sensor. The technical parameters of the UAV used in this study are listed in Table 1. This multi-rotor UAV has several brushless motors, which can provide increased stability and decreased vibration. The information of real-time trajectory and flying altitude, speed, direction, etc. is provided using the inertial measurement unit (IMU) and dual-frequency Global Position System (GPS). The ground control system can track, monitor, and record the UAV flying information continuously. Besides, the Global Navigation Satellite System (GNSS) ground base station is included in the ground control system. In order to guarantee that the accuracy of GPS can reach a steady state, the UAV need to circle the GNSS ground station before automatically executing a scheduled flight mission. The real-time data collected by UAV are sent to the ground data collection terminal and then processed using the state-of-the-art commercial software.

Generation of UAV-LS point clouds

The raw UAV-LS point clouds were obtained using the UAV platform, with a flight speed of 4 m s^{-1} and a flight altitude of 50 m above ground level. The total number of points acquired was approximately 16.16 million, with an average point cloud density of approximately 27,000 pts.m^{-2}. One of the main steps of UAV-LS photogrammetry in UAV-LS photogrammetry module is the generation of UAV-LS point clouds. In order to generate spatially accurate UAV-LS point clouds, the positioning system composed of differential global position system (DGPS) and inertial navigation system (INS) is needed to obtain and update data. Several key

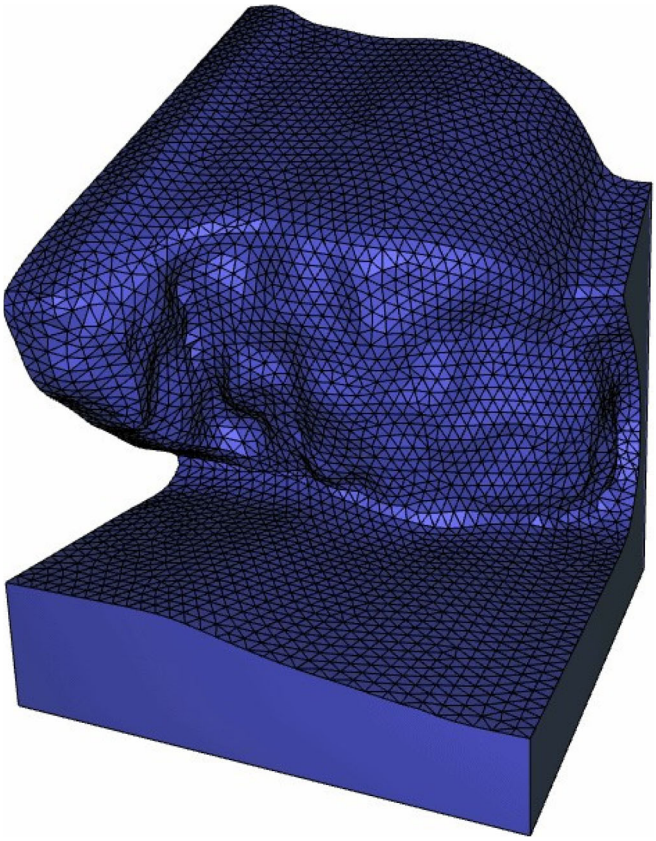

Fig. 6 3D model in DDA user interface

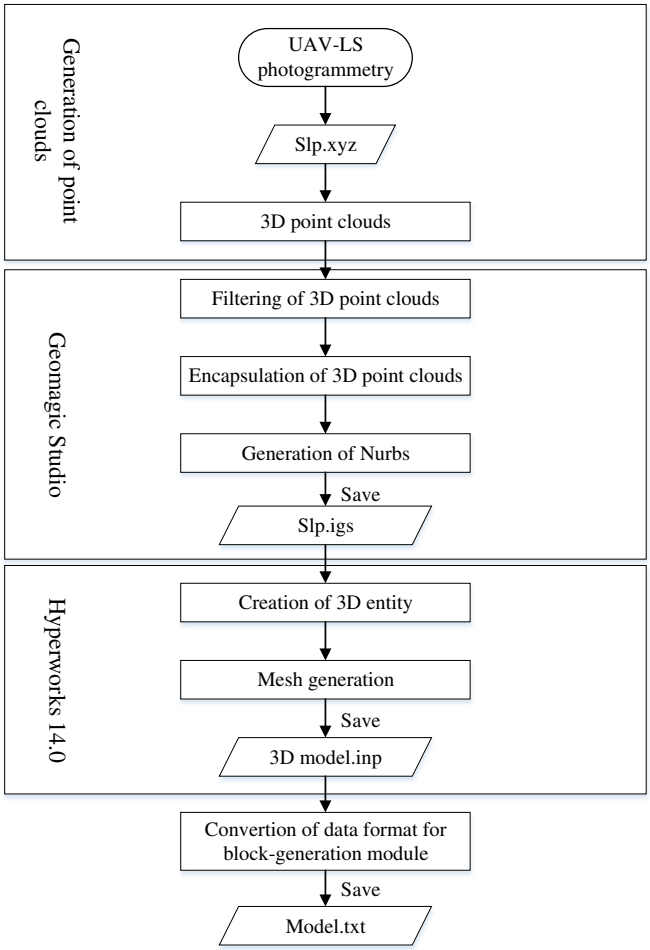

Fig. 7 Process flow chart of generating a 3D model using UAV-LS system and commercial software

steps are as follows: first, in DGPS, GPS data of base station, and UAV platform are integrated using post-processing technique; second, the inertial measurement unit (IMU) data in INS and the processed GPS data obtained from the previous step are combined to produce higher accuracy positioning and trajectory data using Sigma Point Kalman Filter (SPKF) (Crassidis 2006). Finally, the georeferencing UAV-LS equation is used to convert these positioning data into UAV-LS data coordinates as follows:

$$[x, y, z]^T = P_t + R_o(R_b r^s + L_a) \quad (1)$$

where $[x,y,z]^T$ in the mapping frame (North, East, Up) is the coordinates of a point in a given time, P_t is the UAV flight trajectory position at time t, R_o is the direction matrix, R_b and L_a used for system calibration are the boresight matrix and the lever arm, respectively. r^s is the observation matrix of laser scanner, which can be expressed as follows:

$$r^s = \begin{bmatrix} \cos\theta_L & -\sin\theta_L\sin\theta_E & -\sin\theta_L\cos\theta_E \\ 0 & \cos\theta_E & -\sin\theta_E \\ \sin\theta_L & -\cos\theta_L\sin\theta_E & \cos\theta_L\cos\theta_E \end{bmatrix} \begin{bmatrix} 0 \\ 0 \\ r \end{bmatrix} \quad (2)$$

where r is the measured range and θ_L and θ_E are the addition of a layer angle and the encoder angle, respectively. The point cloud data acquired from the UAV-LS system are then transferred to the modeling module. Fig. 1 shows the workflow of generation of UAV-LS point clouds.

Point cloud processing

While the point cloud collected from the UAV-LS system contains accurate geometric information, the data set of point cloud still has many flaws and requires some inevitable processing to create continuous surface models. Point cloud splicing is the most important step of point cloud preprocessing in 3D model reconstruction. In the process of point cloud splicing, the problems are the accumulation of splicing errors and the time-consuming and poor real-time performance. Iterative Closest Point (ICP) algorithm is the most widely used point cloud splicing method (Besl and McKay 1992; Levoy and Rusinkiewicz 2001). However, this algorithm does not fill the hole in the images. Curless and Levoy proposed a volume-space

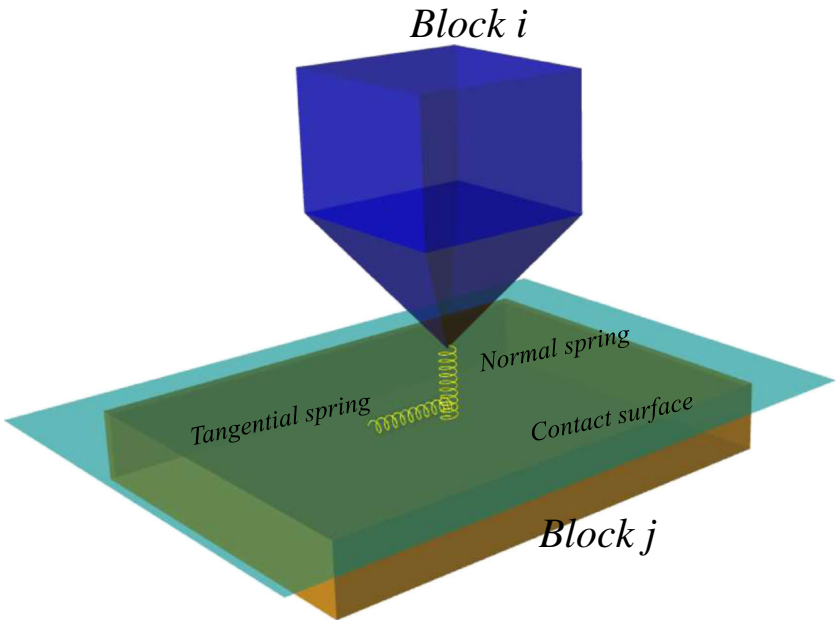

Fig. 8 Contact model between two blocks

fusion matching algorithm, which can not only accurately match high-resolution images from different angles but also fill the holes in the images (Curless and Levoy 1996). Surface reconstruction called Wrap Encapsulation is the next key step after point cloud preprocessing, which, in essence, uses many small spatial triangles to approximate and restore CAD solid model (Edelsbrunner et al. 1998; Edelsbrunner 2003). An algorithm for approximating arbitrary NURBS (non-uniform rational B-spline) curves with bi-arcs is employed to precisely control the curve of the object surface, thus making the 3D model vivid (Piegl and Tiller 2002).

3D modeling

Surface reconstruction based on reverse engineering

The point cloud data of an anti-dip and steep rock slope in small scale from a scenic area in Zhejiang Province, China, is collected using UAV-LS system in the UAV-LS module (Fig. 2). The post-processing of point clouds (Fig. 3) is based on reverse engineering. In a narrow sense, reverse engineering can be defined as the transformation of physical objects into CAD models and then the reconstruction of physical geometric models. The state-of-the-art commercial software named Geomagic Studio used in this paper is a powerful model reconstruction software, which integrates the advantages of efficient point cloud splicing, hole filling, surface reconstruction as well as convenient data format transformation. A series of operations on point clouds in Geomagic Studio are conducted including point cloud denoising (Fig. 4a), encapsulation (Fig. 4b), and NURBS model generation (Fig. 4c). Finally, the model is extended according to the undulation shape at the edge of the slope. The point cloud data file (Slp.xyz) is converted to the NURBS model data file (Slp.igs) that can be processed in the Hyperworks platform.

It is worth noting that LS technique can obtain high-resolution and accurate point cloud data. However, the model processed after the steps above is smoother than the real one, which does not mean that the accuracy and resolution of the model are reduced. One key step of smoothing processing is to generate NURBS model, which has a strong advantage in controlling the curve degree of the object surface thus creating more realistic and vivid models. The purpose of smoothing processing is just reducing the sharpening of the raw model surface thus greatly decreasing the difficulty and workload of subsequent meshing without changing the overall shape and accuracy of the raw model surface. What's more, the stability of rock mass is independent of the roughness of rock mass surface but depends on the properties of the structural planes.

Materialization of 3D model

It is well-known that Hypermesh in the Hyperworks platform has powerful geometric processing capacity and finite mesh division function, which enables it to quickly read data, thus improving the efficiency and quality of finite element mesh division. In the Hyperworks platform, operations including the creation of 3D entity, the Boolean operations, the trimming of 3D model, and the mesh generation are conducted. In order to facilitate the pre-processing of 3D-DDA, only the upper surface of the 3D model is meshed (Fig. 5). The NURBS model data file (Slp.igs) is finally converted to 3D model data

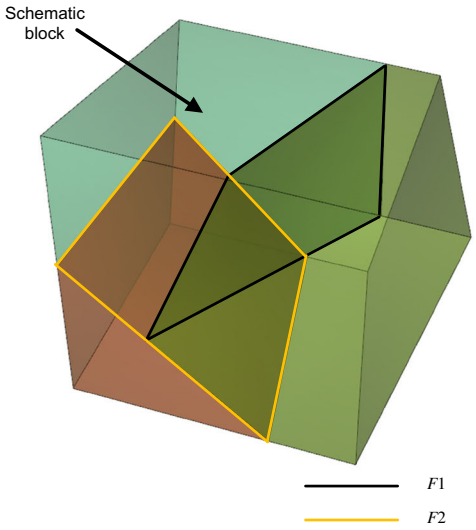

(a) Finite structural planes

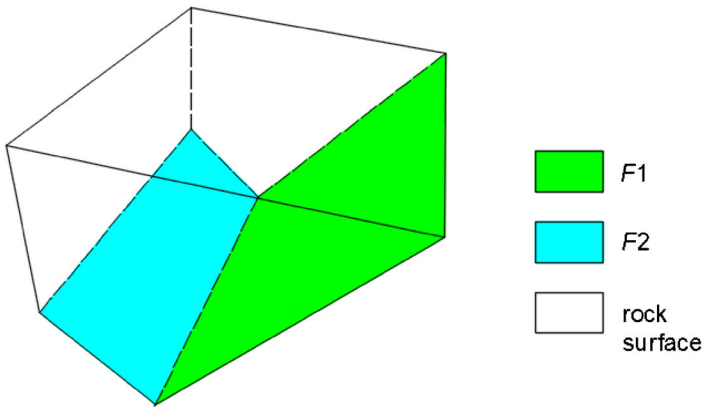

(b) Generation of a schematic block from a

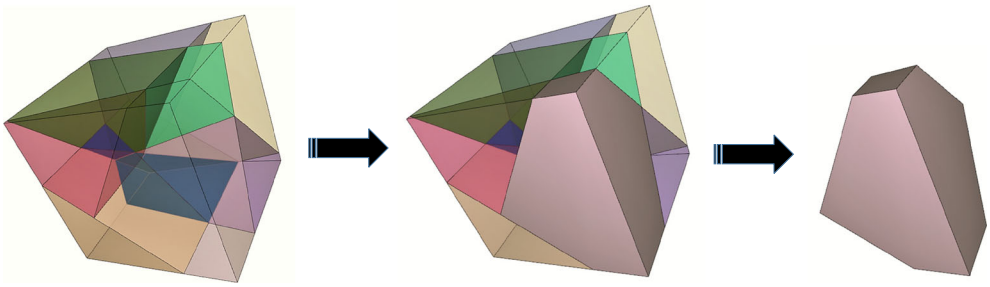

(c) Blocks with arbitrary shapes

Fig. 9 Generation of blocks using block-cutting algorithm

file (3D model.inp) that can then be easily processed into the data file (Model.txt) for the subsequent 3D-DDA pre-processing in the modeling module. The 3D model can be displayed in DDA user interface (Fig. 6). Figure 7 shows the process flow chart of generating 3D model using UAV-LS system and state-of-the-art commercial software.

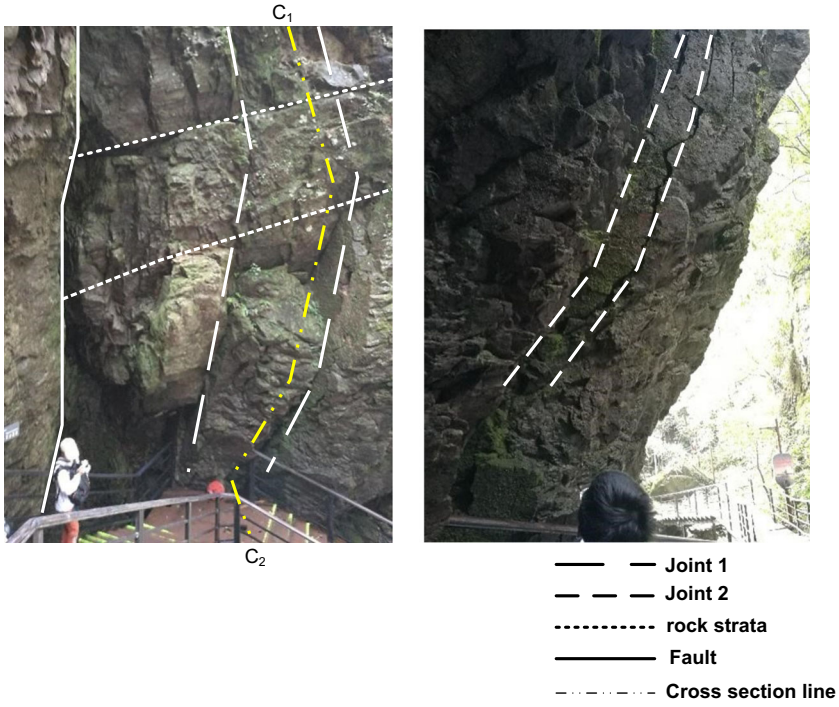

Fig. 10 Structural planes from geological investigations

Method of 3D discontinuous model generation

3D-DDA theory

3D-DDA is a numerical simulation method that solves the grid of finite element which is similar to FEM. The problem is solved where rock mass is divided into blocks of arbitrary shapes by the pre-existing discontinuous structural planes such as joints and faults. The blocky system is formed by the mutual contact and displacement constraints between several blocks. Similar to FEM, the global governing equation is derived from the principle of minimum potential energy. In each small time step, the displacement increment of the block is relatively small. Therefore, the displacement function of blocks can be represented reasonably by the first-order approximation.

The first-order approximation of the displacement function is assumed to be in constant stress and strain state at each time step. $[u\ v\ w]^T$ is derived as shown in Eq. (3), for a n block system (Shi 2001):

$$[u\ \ v\ \ w]^T = [T_i(x,y,z)][D_i] \tag{3}$$

$$[T_i(x,y,z)] = \begin{bmatrix} 1 & 0 & 0 & -(y-y_c) & 0 & (z-z_c) & (x-x_c) & 0 & 0 & \frac{(y-y_c)}{2} & 0 & \frac{(z-z_c)}{2} \\ 0 & 1 & 0 & (x-x_c) & -(z-z_c) & 0 & 0 & (y-y_c) & 0 & \frac{(x-x_c)}{2} & \frac{(z-z_c)}{2} & 0 \\ 0 & 0 & 1 & 0 & (y-y_c) & -(x-x_c) & 0 & 0 & (z-z_c) & 0 & \frac{(y-y_c)}{2} & \frac{(x-x_c)}{2} \end{bmatrix} \tag{4}$$

Table 2 The orientation of the structural planes and the slope

ID	Dip direction(°)	Dip angle(°)
Slope	225	80
Rock strata	225	9
Joint 1	309	78
Joint 2	230	81
Fault	311	89

$$[D_i]^T = \begin{bmatrix} u_c & v_c & w_c & r_x & r_y & r_z & \varepsilon_x & \varepsilon_y & \varepsilon_z & \gamma_{xy} & \gamma_{yz} & \gamma_{zx} \end{bmatrix} \tag{5}$$

where (x, y, z) is the displacement of an arbitrary point in block i; (x_c, y_c, z_c) is the centroid coordinates of block i; $[T_i(x, y, z)]$ is the displacement transformation matrix of block i; (u_c, v_c, w_c) is the translational displacement; (r_x, r_y, r_z) is the rotational

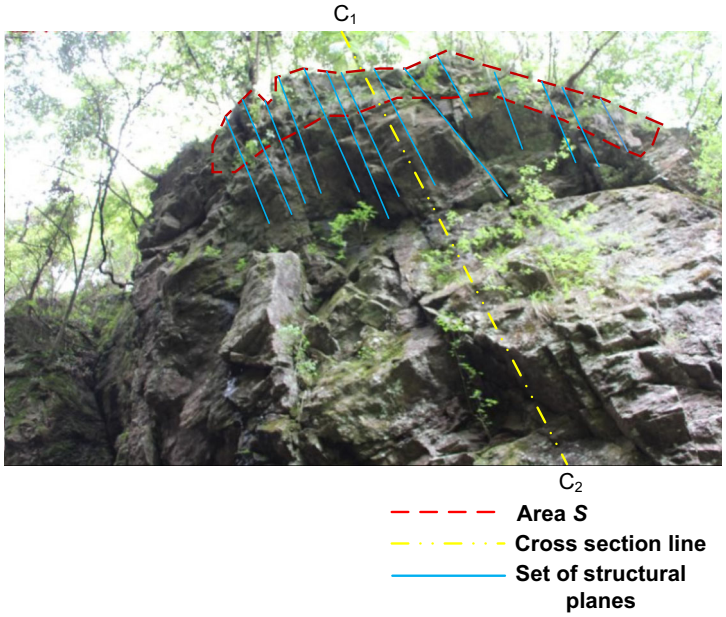

(a) Potentially unstable area and cross section line

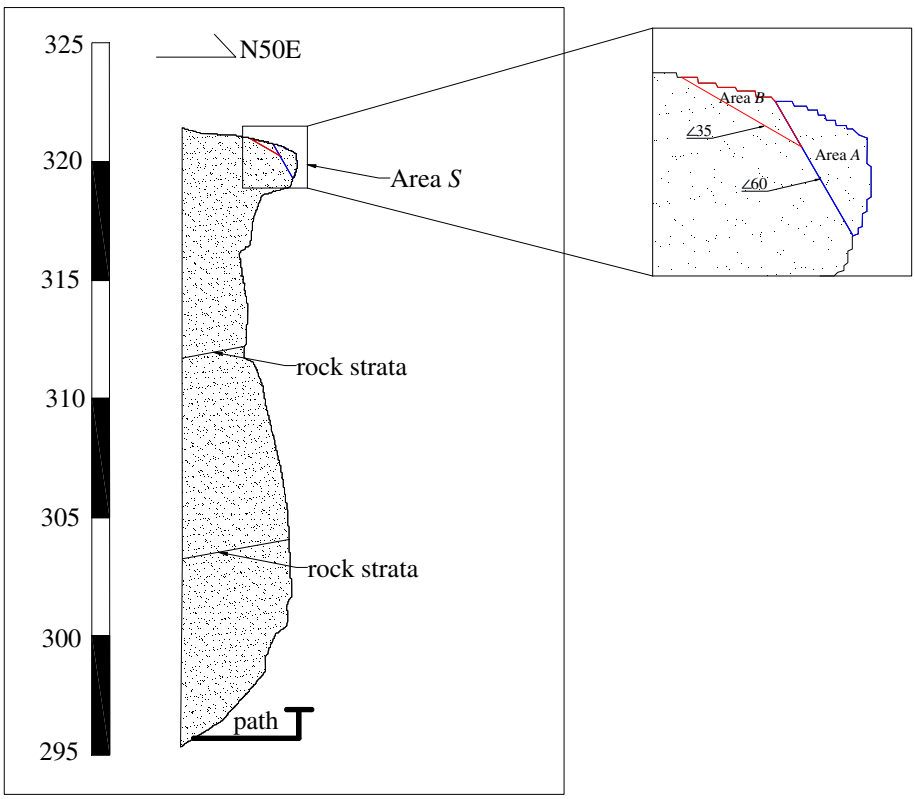

(b) Cross-section with discontinuities

Fig. 12 Generation of geological cross section based on ArcGIS. The potentially unstable Area *S* is controlled by discontinuities in a and b

displacement; and (ε_x, ε_y, ε_z) and (γ_{xy}, γ_{yz}, γ_{zx}) are the normal strain and the tangential strain, respectively.

The global governing equation of DDA is derived by minimizing the summation of potential energy of block system which is

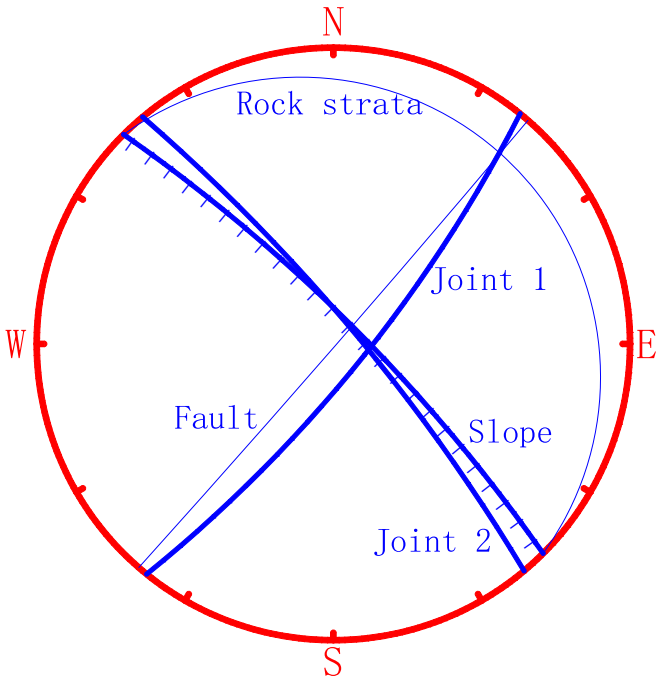

Fig. 11 Stereographic projection of the main sets of the structure planes and the slope

obtained by taking partial derivatives of each deformation variable of n block system as in Eq. (6):

$$\begin{bmatrix} K_{11} & K_{12} & K_{13} & \cdots & K_{1n} \\ K_{21} & K_{22} & K_{23} & \cdots & K_{2n} \\ K_{31} & K_{32} & K_{33} & \cdots & K_{3n} \\ \vdots & \vdots & \vdots & \vdots & \vdots \\ K_{n1} & K_{n2} & K_{n3} & \cdots & K_{nn} \end{bmatrix} \begin{bmatrix} D_1 \\ D_2 \\ D_3 \\ \vdots \\ D_n \end{bmatrix} = \begin{bmatrix} F_1 \\ F_2 \\ F_3 \\ \vdots \\ F_n \end{bmatrix} \quad (6)$$

where $[D_i]$ and $[F_i]$ are 12×1 vector displacement variable and loading submatrix related to external forces and internal stresses acting on block i, respectively; $[K_{ii}]$ is 12×12 vectors stiffness submatrix depending on properties of materials of block i since each block i has 12 degrees of freedom; $[K_{ij}]_{i \neq j}$ is defined by the contact between block i and block j.

In the 3D-DDA method, the penalty function is used to prevent blocks from being interpenetrated. There are three types of contact states between blocks, that is: locked, sliding, and open. When the blocks are in contact with each other and are about to interpenetrate, a deformable spring is added to the contact position to prevent interpenetration both in normal and tangential directions (Fig. 8). The open-close iteration (OCI) (Shi 1988) is used to meet the condition of no tension and no interpenetration at each time step. The shear stress on the boundary when the blocks are in contact obeys the failure criterion of Mohr-Coulomb as follows:

If $k_n d_n > 0$ and $k_s d_s \leq k_n d_n \tan\phi + cA$, the blocks are considered to be locked with each other; if $k_n d_n > 0$ and $k_s d_s > k_n d_n \tan\phi + cA$, the blocks are considered to slide over the surface of other blocks; if $k_n d_n < 0$, the blocks are considered to be open, where k_n and k_s are the stiffness of springs in the normal and tangential directions, respectively; d_n and d_s are the interpenetration distance of blocks in the normal and tangential directions; the cohesion c and the friction angle ϕ are the mechanical parameters of structural planes; A is the contact area between blocks.

Generation of 3D discontinuous blocks

In DDA method, the discontinuous model is generated by the spatial distribution of structural planes such as faults and joints. The block-cutting algorithm used in the block-generation module is an improved and independent algorithm based on the code proposed by Peng (Peng and Pei 1992), which enables it to cut blocks directly from 3D topography. The feature of this algorithm lies in the fact that it can search for blocks directly from the 3D network of structural planes and rock surfaces without considering the pyramid body in block theory, thus making the generation of concave blocks possible. In this algorithm, the cutting plane is regarded as a circular face with a finite radius by mutual constraints between the structural planes. Figure 9a shows that the structural plane F_1 is truncated by the structural plane F_2, thus making F_1 become finite in size. The problem that the structural planes are finite planes is solved using this method, which is more consistent with practical engineering, compared with the assumption that structural surface is infinite in 3D-DDA proposed by Shi (1988). A method of representing a block by a closed space surrounded structural planes F_1 and F_2 and existing rock surfaces such as slope face are displayed (Fig. 9b). Figure 9c shows the process of generating complex blocks with arbitrary structural planes using this algorithm.

In fact, the block-cutting algorithm is a kind of mathematical geometric topology method. It combines the geometric equation of network with the topological relation of block elements, which is simple and feasible. The position, dip direction, and dip angle of discontinuities are executed by the block-cutting algorithm to generate blocky model and then transmitted to the 3D-DDA

Table 3 Material properties and physical parameters in simulation of a blocky rock mass slope

Description	Notation	Value
Density	ρ (kg/m^3)	2500
Poisson's ratio	ν	0.25
Elastic modulus	E (GPa)	3.5
Normal contact spring stiffness	k_n (kN/m)	2.0×10^8
Tangential contact spring stiffness	k_s (kN/m)	2.0×10^7
Cohesion	c (MPa)	0.5
Friction angle	ϕ (°)	35
Gravity acceleration	g (m/s^2)	− 10
Time interval	Δt (s)	0.0001
Total time steps	N	250,000

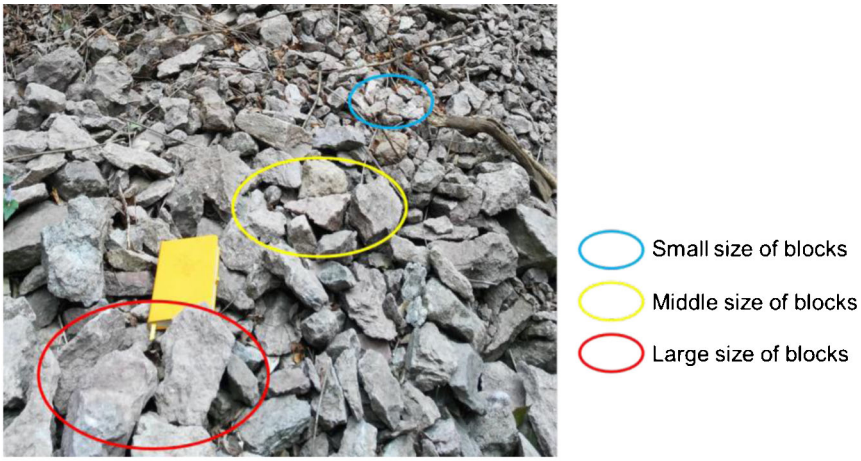

(a) The fragmental rockfalls detached from the upper section of the slope vary in size and shape relatively.

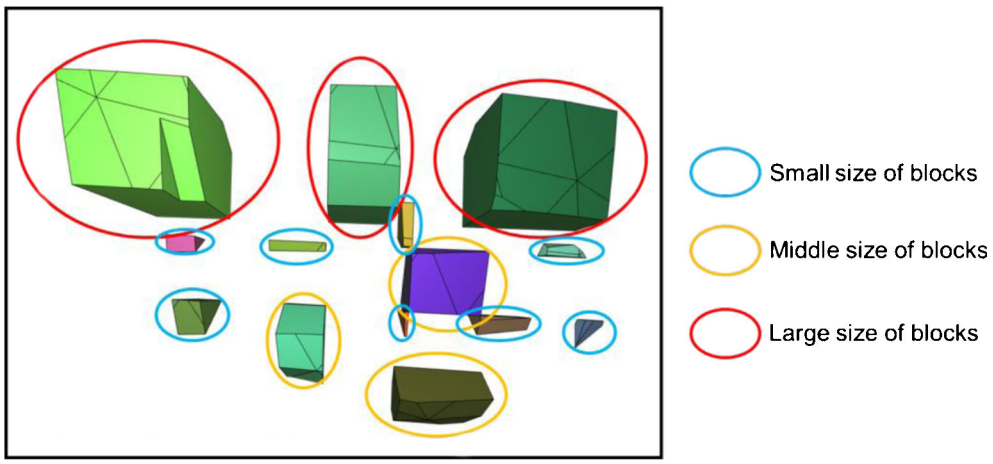

(b) The blocks with arbitrary shapes from the crushed Area *S* are generated using the block cutting scheme.

Fig. 13 Example of the fragmental rockfalls in **a** is not exactly the same as the blocks in **b**, but the arbitrariness of the size and shape of blocks in **a** and **b** indicates that they are generally similar

calculation module. Figure 9c shows the process of generating blocks with arbitrary shapes cut by complex structural planes.

Numerical example

Overview

The slope selected for stability analysis is an anti-dip and steep rock slope from a scenic area in Zhejiang Province, China. The slope is located next to a spectacular waterfall, which usually attracts a lot of visitors. According to geological investigations, the rock mass is relatively fragmented and mainly controlled by four groups of structural planes (Fig. 10) plotted in the stereographic projection (Fig. 11). The rock mass is cut by the 3D network consisting of the well-developed rock strata, a fault, Joint 1 and Joint 2. The orientation of the structural planes and the slope is summarized in Table 2. A cross section is implemented in order to demonstrate detailed 3D model. Point cloud data of the intersection line C_1–C_2 between cross section and slope face extracted based on ArcGIS geoprocessing technology are employed to generate the cross section (Fig. 12b) with CAD technology. It is evident that Area *S* in the upper section of the slope is heavily wooded (Fig. 12a). Root wedging is obvious due to roots of trees growing along cracks and joints, thus making Area *S* extremely fragmented and potentially unstable. According to field surveys, Area *S* is

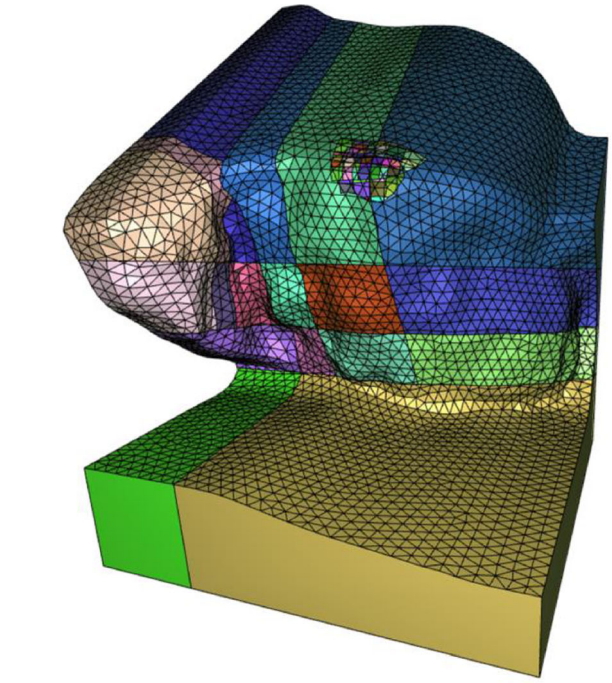

(a) 3D block model with surface grids

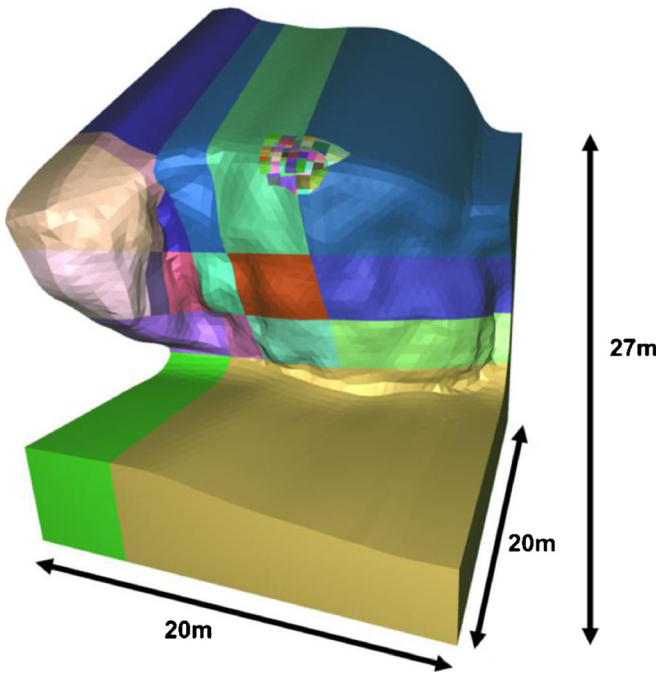

(b) 3D block model without surface grids

Fig. 14 Generation of 3D blocky model using block-cutting algorithm

dominated by two main structural planes whose dip angles are approximately 35° and 60°, respectively, based on which Area *S* is divided into two areas: Area *A* and Area *B* (Figs. 12b and 15). The cracks in Area *S* mostly follow the structural planes shown in Fig. 12a. The rocks between the cracks are relatively fragmented, similar to the rockfalls piled up at the site (Fig. 13a). According to the introduction of scenic area personnel, at the present time, Area *S*, especially Area *A*, is the place where relatively frequent rockfalls occur. It has been observed that rockfalls occur when it rains in the scenic spot.

3D discontinuous model generation

3D blocky model is generated using the block-cutting algorithm according to the main joints (Figs. 10 and 12). The block-cutting scheme adopted in Area *S* is based on the set of the structural planes shown in Fig. 12. The rockfalls at the site in Fig. 13a are generally similar to the blocks in Fig. 13b due to the arbitrariness of the size and shape of blocks, though they are not exactly the same, which indicates that the block-cutting scheme is valid to some extent. The anti-dip slope model has a length of 20 m, a width of 20 m, and a height of 27 m (Fig. 14). The material properties and physical parameters in simulation of a slope in blocky rock mass are given in Table 3. The physical parameters used in this paper are based on a geological disaster survey project of Shenxianju scenic area in Zhejiang province. The mechanical parameters of the structural planes and rock mass are obtained by field rebound test, field mapping combined with laboratory experiments of rock mechanics after conducting field sampling. The value of contact stiffness is obtained according to the motion of blocks after calculation. The corresponding stiffness is adjusted and considered to be reasonable until there are no abnormal phenomena such as obvious intrusion and jumping of blocks. Several assumptions have been considered based on the code adopted in this study, namely the following: (a) all the structural planes are flat and transfixion planes and (b) are of zero thickness without considering its spacing.

After implementing the block-cutting algorithm, 3D blocky model consisting of 131 blocks is generated (Fig. 14). Constraints are then applied on the front, back, left, right, and bottom of the model.

Calculation and analysis with 3D-DDA

The 3D-DDA calculation module is an optimized code developed by the authors. The simulation results (Fig. 16) after calculating in the 3D-DDA calculation module indicate that the unstable blocks mainly come from the upper section of the rock mass, which reveal that the anti-dip rock slope is globally stable with local sliding failure. The two potentially unstable areas *A* and *B* (Fig. 15) can be marked based on the numerical result analysis. The Area *A* denotes a zone with a sliding failure along the shallow structural plane with a large dip angle 60°, where rockfalls occur frequently. The initial movement of the first sliding block in Area *A*, usually considered as a key block, occurs in the first 2.5 s. Thereafter, other blocks in Area *A* also moves along the structural plane. Subsequently, the moving blocks gradually fall down under the action of gravity and collide with the model base. The kinematic characteristics of blocks vary greatly due to their different geometric shapes. The stability analysis indicates that the upper section of this slope is in an unstable state, which is consistent with the real situation.

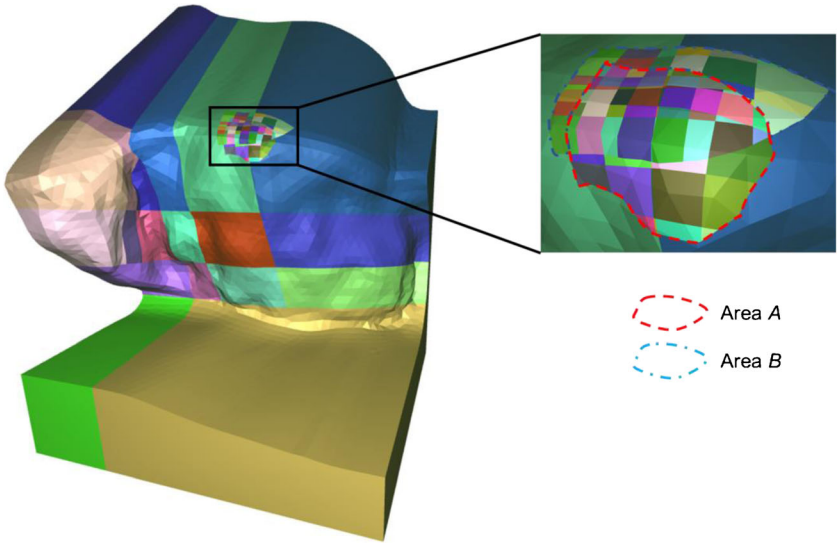

Fig. 15 Division of unstable areas *A* and *B*

The Area *B* denotes a zone where blocks are relatively stable at present though the stability margin is a little bit small (Fig.18a). As can be seen from the ultimate simulation results (Fig. 16), blocks in Area *B* in the overlapping section of Area *A* and Area *B* also move without the hindrance of blocks in Area *A* at the end of the simulation. It indicates that some local rockfalls do occur frequently in the intersection area between Area *A* and Area *B*, though large sliding failure is of very low likelihood at this moment.

In order to further analyze the stability of Area *B*, this paper uses the Strength Reduction Method (SRM) to estimate the safety of the slope. In real cases, this scenic area in Zhejiang Province is rich in rain especially in summer. When it rains, the rainwater moves along the discontinuities of fragmented rock mass and washes away the filling and cementing between discontinuous surfaces, which can usually reduce the mechanical parameters c and ϕ correspondingly and induce further rock mass displacement and deformation. The sliding failure of fragmented rock mass usually occurs along the discontinuities. Therefore, SRM is an easy and direct method to analyze the stability of the slope. The essence of SRM is that the cohesion c and the internal friction angle ϕ of the blocks and joints decrease gradually. To be specific, a series of new strength parameters c' and ϕ', divided by a shear strength reduction factor F_s, respectively, are obtained as in Eq. (7):

$$c' = \frac{c}{F_s} \qquad \phi' = \arctan\left(\frac{\tan\phi}{F_s}\right) \tag{7}$$

With the increasing shear strength reduction of the factor F_s, the shear strength gradually decreases until a certain shear strength is reached to a point at which the instability of the slope occurs. At this very moment, the shear strength reduction factor is considered as the minimum safety factor of the slope, which is equal to the safety factor obtained by the limit equilibrium method (LEM).

The stability analysis of the numerical example is implemented using the SRM-based 3D-DDA. According to the laboratory test of rock mechanics parameters, the cohesion c is relatively small. Thus, in this paper, SRM is applied only for the internal friction angle without reducing the cohesion force. Different values of the internal friction angle obtained by SRM are 30°, 25°, and 20°. The corresponding strength reduction factors are 1.17, 1.40, and 1.75, respectively. From the simulation results (Fig. 18), blocks in Area *A* where rockfalls occur frequently, are unstable in any cases, since this area is controlled by a structural plane with a large dip angle approximately 60°. It is worth noting that the stability of rock mass depends on the properties of the structural planes. Indeed, each set of planes would have different characteristics, thus making c and ϕ different. However, the slope studied in this paper is stable except Area *S* and this is the actual situation. Besides, the overall stability of the slope except Area *S* cannot be changed by applying the parameters of any structural plane shown in Figs. 11 and 12 according to the constraints of the model.

However, the stability of fragmented rock mass in Area *B* varies with different strength reduction factors. Block #96 from Area *B* is selected in this paper to record its displacement history (Fig. 17). When the internal friction angle is 35°, the displacement in the x, y, and z directions of Block #96 is nearly zero (Figs. 18a and 19a), which indicates that Area *B* is in the critical state of relative sliding and the corresponding safety factor is approximately 1.0. When the internal friction angle is 30°, the maximum moving distance of Block #96 in the z direction is 12 cm, which means that sliding failure occurs among blocks in Area *B*. It is evident that the moving distance of blocks in Area *B* increases with the decreasing of internal friction angle (Figs. 18 and 19). When the internal friction angle decreases to 20°, almost all the blocks in Area *B* fall

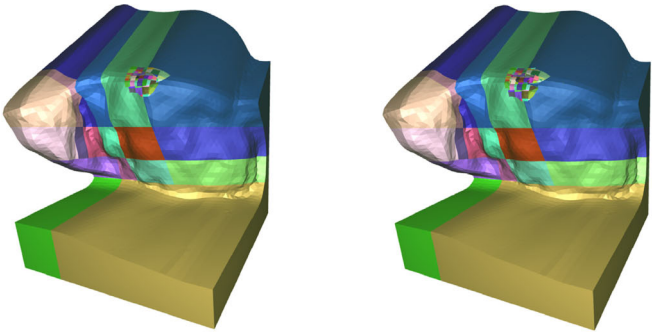

(a) t=0.0s (b) t=4.1s

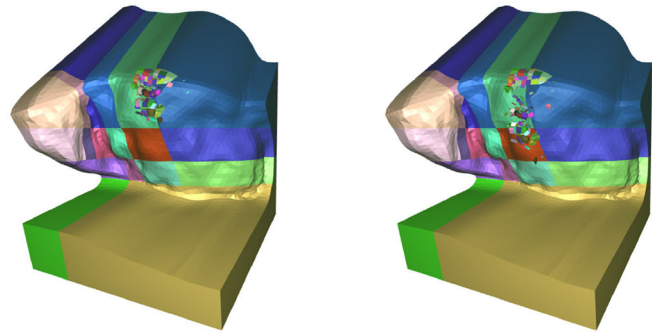

(c) t=8.3s (d) t=12.5s

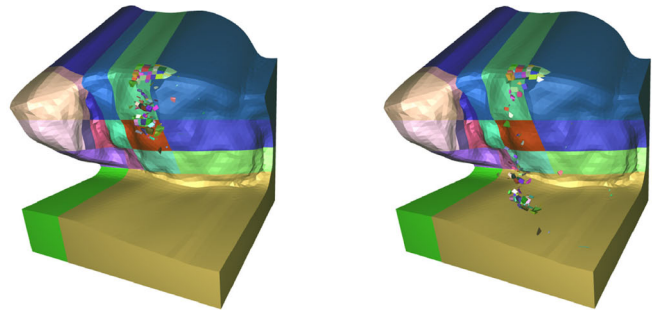

(e) t=17.1s (f) t=21.1s

Fig. 16 Failure simulation sequences of the blocky slope

down from the upper section of the slope (Fig. 18d), thus making Area *B* completely unstable.

The slope in blocky rock mass selected in this paper is controlled by obvious discontinuities (joints, faults) and the upper section Area *S* is mainly characterized by the cataclastic structure, which is easy to break away from the parent rock under the action of external forces such as gravity. In the practical situation (Fig. 13a), the rocks fall off from the upper section of the slope and pile up on the ground which coincide with the simulation results. At present, Area *B* is relatively stable and safe. However, the sliding of blocks in Area *B* will be of high probability to initiate if adverse conditions such as strong rainfalls and seismic activities occur.

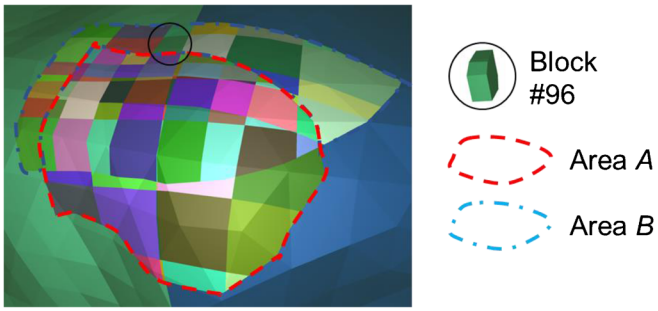

Fig. 17 Block #96 is used to record the displacement history

Conclusions and Discussion

3D simulation and stability analysis of blocky rock slope considering the spatial effects are very significant in the aspect of risk assessment and disaster prevention in practical engineering cases. In this study, the system that combines the UAV-LS photogrammetry with 3D-DDA is successfully applied for stability analysis of a blocky assembly. The simulation results indicate that this system is capable of providing a solution for efficient 3D modeling and stability analysis of blocky rock slope. This system contains the UAV-LS photogrammetry module, the modeling module, the block-generation module, and the 3D-DDA calculation module.

The primary characteristics of this system can be summarized as follows: (1) the point cloud data obtained by UAV-LS photogrammetry is convenient and time saving for data conversion and processing based on the Geomagic Studio and Hyperworks platforms; (2) an independent block-cutting algorithm is used in the block-generation module, which enables it to cut blocks directly from 3D topography and generate a large number of blocks with arbitrary shapes; (3) the problem that the structural plane is finite is solved using the block-cutting algorithm, which is more consistent with practical engineering cases; and (4) a user-friendly interface in the 3D-DDA calculation module is used to simulate the dynamic movement of blocks and locate the unstable section and accumulation zone.

UAV systems are increasingly considered to be the preferred choice due to the fact that they are nearly the most inexpensive aerial option and can also provide the maximum capability of avoiding occlusions when dealing with high and steep slopes. In addition, LS technique is fast and extremely precise with the detailed geometric features of geologic bodies. However, some problems to be addressed in the future still exist. The combination of UAV and LS decreases the precision and resolution of point cloud data to a certain degree when compared to single technique and ground-based platforms such as hand-held devices, tripods. Besides, weather conditions such as rainy or windy days can restrict the use of UAV-LS technique. In some regions, UAV regulations may restrict or preclude the use of UAVs. Nevertheless, it should be emphasized that wherever possible, remote sensing approaches should be supplemented with photographic site observations and field mapping. Therefore, the system and method proposed in this paper is believed to be as a solid foundation for rapid 3D simulation and stability analysis of practical engineering cases.

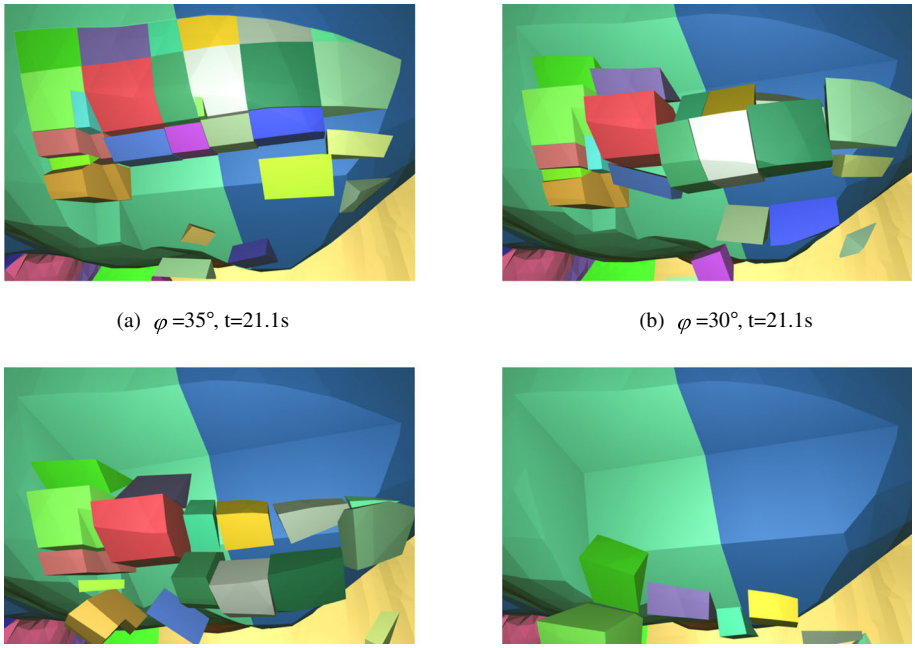

(a) φ =35°, t=21.1s (b) φ =30°, t=21.1s

(c) φ =25°, t=21.1s (d) φ =20°, t=21.1s

Fig. 18 Ultimate failure modes of Area *A* and Area *B* using SRM with different internal friction angles

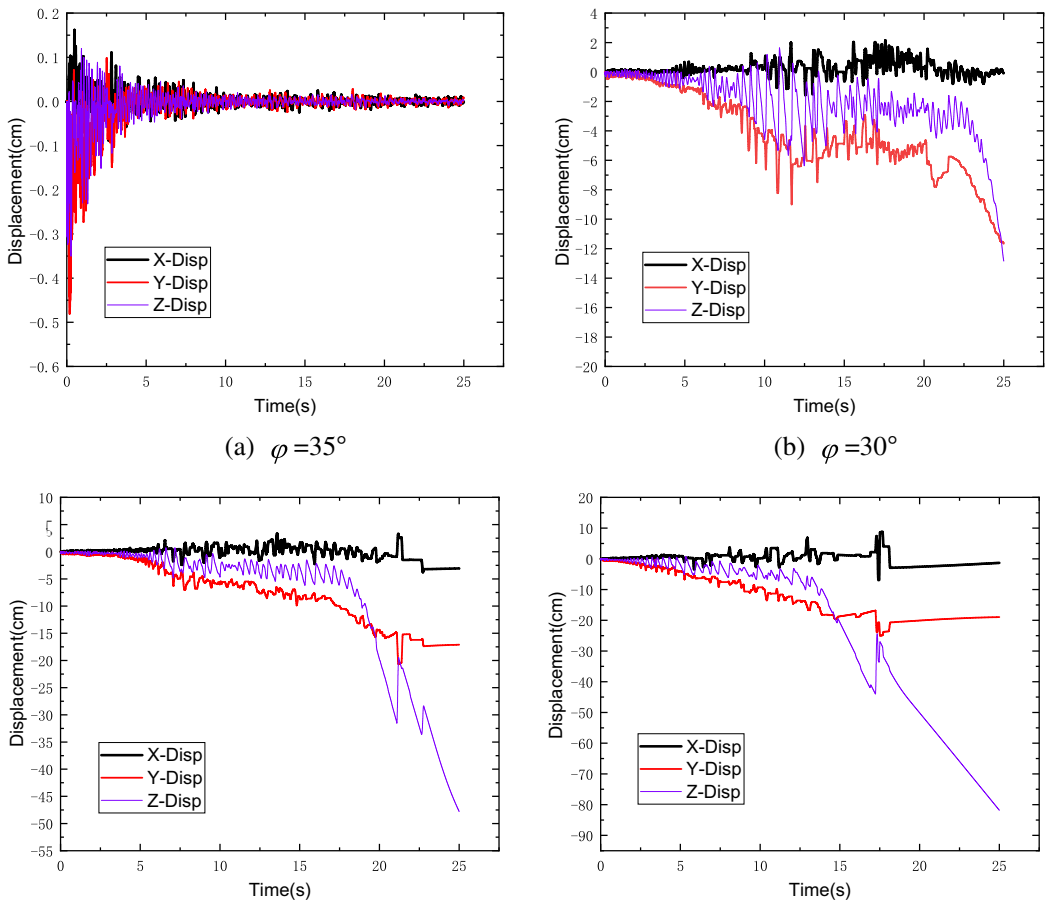

(a) φ =35° (b) φ =30°

(c) φ =25° (d) φ =20°

Fig. 19 Displacement history of Block #96

Acknowledgements

The National Key Research and Development Plan (Grant No. 2018YFC1504801, 2018YFC1504902), the National Natural Science Foundation-Outstanding Youth Foundation (Grant No. 51522903), National Natural Science Foundation of China (Grant No. 51479094, 41772246), and the Open Research Fund Program of the State Key Laboratory of Hydroscience and Engineering (Grant No. 2016-KY-02 and 2016-KY-05) are gratefully acknowledged.

References

Besl P, McKay N (1992) A method for registration of 3-D shapes. IEEE Trans Pattern Anal Mach Intell 14:239–256. https://doi.org/10.1109/34.121791

Beyabanaki SAR, Mikola RG, Hatami K (2008) Three-dimensional discontinuous deformation analysis (3-D DDA) using a new contact resolution algorithm. Comput Geotech 35:346–356. https://doi.org/10.1016/j.compgeo.2007.08.006

Bonilla-Sierra V, Scholtès L, Donzé FV, Elmouttie MK (2015) Rock slope stability analysis using photogrammetric data and DFN–DEM modelling. Acta Geotech 10:497–511. https://doi.org/10.1007/s11440-015-0374-z

Cai Y, Zhu H, Zhuang X (2013) A continuous/discontinuous deformation analysis (CDDA) method based on deformable blocks for fracture modeling. Front Struct Civ Eng 7:369–378. https://doi.org/10.1007/s11709-013-0222-x

Cervera M, Barbat GB, Chiumenti M (2017) Finite element modeling of quasi-brittle cracks in 2D and 3D with enhanced strain accuracy. Comput Mech 60:767–796. https://doi.org/10.1007/s00466-017-1438-8

Chen G (2003) Numerical modelling of rock fall using extended DDA. J Rock Mech Eng (in Chinese) 22:926–931

Chen G, Zheng L, Zhang Y, Wu J (2013) Numerical simulation in rockfall analysis: a close comparison of 2-D and 3-D DDA. Rock Mech Rock Eng 46:527–541. https://doi.org/10.1007/s00603-012-0360-9

Clayton A, Stead D, Kinakin D, Wolter A (2017) Engineering geomorphological interpretation of the Mitchell Creek landslide, British Columbia, Canada. Landslides 14:1655–1675. https://doi.org/10.1007/s10346-017-0811-1

Coggan J, Wetherelt A, Gwynn X, Flynn Z (2007) Comparison of hand-mapping with remote data capture systems for effective rock mass characterisation, vol 1

Crassidis JL (2006) Sigma-point Kalman filtering for integrated GPS and inertial navigation. IEEE Trans Aerosp Electron Syst 42:750–756. https://doi.org/10.1109/TAES.2006.1642588

Curless B, Levoy M (1996) A volumetric method for building complex models from range images. International Conference on Computer Graphics and Interactive Techniques. pp 303–312. https://doi.org/10.1145/237170.237269

Donati D, Stead D, Brideau MA, Ghirotti M (2017) A remote sensing approach for the derivation of numerical modelling input data: insights from the Hope slide, Canada.

Edelsbrunner H (2003) Surface reconstruction by wrapping finite sets in space Discret Comput Geom 379–404. https://doi.org/10.1007/978-3-642-55566-4_17.

Edelsbrunner H, Facello MA, Fu P, Qian J, Nekhayev DV (1998) Wrapping 3D scanning data. In: Proc SPIE Int Soc Opt Eng, vol 3313, pp 148–158. https://doi.org/10.1117/12.302448

Fakhimi A, Carvalho F, Ishida T, Labuz JF (2002) Simulation of failure around a circular opening in rock. Int J Rock Mech Min Sci 39:507–515. https://doi.org/10.1016/S1365-1609(02)00041-2

Fan H, Zheng H, Wang J (2018) A generalized contact potential and its application in discontinuous deformation analysis. Comput Geotech 99:104–114. https://doi.org/10.1016/j.compgeo.2018.02.023

Firpo G, Salvini R, Francioni M, Ranjith PG (2011) Use of digital terrestrial photogrammetry in rocky slope stability analysis by distinct elements numerical methods. Int J Rock Mech Min Sci 48:1045–1054. https://doi.org/10.1016/j.ijrmms.2011.07.007

Francioni M, Salvini R, Stead D, Litrico S (2014) A case study integrating remote sensing and distinct element analysis to quarry slope stability assessment in the Monte Altissimo area, Italy. Eng Geol 183:290–302. https://doi.org/10.1016/j.enggeo.2014.09.003

Francioni M, Salvini R, Stead D, Giovannini R, Riccucci S, Vanneschi C, Gullì D (2015) An integrated remote sensing-GIS approach for the analysis of an open pit in the Carrara marble district, Italy: slope stability assessment through kinematic and numerical methods. Comput Geotech 67:46–63. https://doi.org/10.1016/j.compgeo.2015.02.009

Ghirotti M, Genevois R (2007) A complex rock slope failure investigated by means of numerical modelling based on laser scanner technique. Paper presented at the 1st Canada - U.S. Rock Mechanics Symposium, Vancouver, Canada, 2007/1/1/

Haneberg W, Norrish N, Findley D (2006) Digital outcrop characterization for 3D structural mapping and rock slope design along interstate 90 near Snoqualmie pass, Washington

Havaej M, Coggan J, Stead D, Elmo D (2016) A combined remote sensing–numerical modelling approach to the stability analysis of Delabole Slate Quarry, Cornwall, UK. Rock Mech Rock Eng 49:1227–1245. https://doi.org/10.1007/s00603-015-0805-z

Hazzard JF, Young RP (2000) Simulating acoustic emissions in bonded-particle models of rock. Int J Rock Mech Min Sci 37:867–872. https://doi.org/10.1016/S1365-1609(00)00017-4

He L, Ma GW (2010) Development of 3D numerical manifold method. Int J Comput Methods 07:107–129. https://doi.org/10.1142/s0219876210002088

Jiang QH, Yeung MR (2004) A model of point-to-face contact for three-dimensional discontinuous deformation analysis. Rock Mech Rock Eng 37:95–116. https://doi.org/10.1007/s00603-003-0008-x

Jiang QH, Chen Y, Zhou C, Yeung MR (2013) Kinetic energy dissipation and convergence criterion of discontinuous deformations analysis (DDA) for geotechnical engineering. Rock Mech Rock Eng 46:1443–1460. https://doi.org/10.1007/s00603-012-0356-5

Kaidi S, Rouainia M, Ouahsine A (2012) Stability of breakwaters under hydrodynamic loading using a coupled DDA/FEM approach. Ocean Eng 55:62–70. https://doi.org/10.1016/j.oceaneng.2012.07.035

Kazerani T, Yang ZY, Zhao J (2012) A discrete element model for predicting shear strength and degradation of rock joint by using compressive and tensile test data. Rock Mech Rock Eng 45:695–709. https://doi.org/10.1007/s00603-011-0153-6

Keneti AR, Jafari A (2008) Determination of volume and centroid of irregular blocks by a simplex integration approach for use in discontinuous numerical methods. Geomech Geoeng 3:79–84. https://doi.org/10.1080/17486020701730041

Lato M, Diederichs M, Hutchinson D, Harrap R (2009) Optimization of LiDAR scanning and processing for automated structural evaluation of discontinuities in rockmasses, vol 46. https://doi.org/10.1016/j.ijrmms.2008.04.007

Levoy M, Rusinkiewicz S (2001) Efficient variants of the ICP algorithm. 3D Digital Imaging and Modeling. pp 145–152

Ma G, Matsuyama H, Nishiyama S, Ohnishi Y (2011) Practical studies on rockfall simulation by DDA. J Rock Mech Geotech Eng 3:57–63. https://doi.org/10.3724/SP.J.1235.2011.00057

Mantovani M, Devoto S, Piacentini D, Prampolini M, Soldati M, Pasuto A (2016) Advanced SAR interferometric analysis to support geomorphological interpretation of slow-moving coastal landslides (Malta, Mediterranean Sea) vol 8. https://doi.org/10.3390/rs8060443

Niethammer U, James MR, Rothmund S, Travelletti J, Joswig M (2012) UAV-based remote sensing of the Super-Sauze landslide: evaluation and results. Eng Geol 128:2–11. https://doi.org/10.1016/j.enggeo.2011.03.012

Peng XC, Pei JM (1992) Simulation of 3-D discontinuity network and analysis of key block in rock slope. Tsinghua University (in Chinese)

Piegl L, Tiller W (2002) Biarc approximation of NURBS curves. Comput Aided Des 11:807–814. https://doi.org/10.1016/S0010-4485(01)00160-9

Riquelme A, Cano M, Tomás R, Abellán A (2017) Identification of rock slope discontinuity sets from laser scanner and photogrammetric point clouds: a comparative analysis. Proced Eng 191:838–845. https://doi.org/10.1016/j.proeng.2017.05.251

Riquelme A, Soldato MD, Tomás R, Cano M, Bordehore LJ, Moretti S (2019) Digital landform reconstruction using old and recent open access digital aerial photos. Geomorphology 329:206–223. https://doi.org/10.1016/j.geomorph.2019.01.003

Salvini R, Francioni M, Riccucci S, Fantozzi PL, Bonciani F, Mancini S (2011) Stability analysis of "Grotta delle Felci" cliff (Capri Island, Italy): structural, engineering–geological, photogrammetric surveys and laser scanning. Bull Eng Geol Environ 70:549–557. https://doi.org/10.1007/s10064-011-0350-2

Salvini R, Francioni M, Riccucci S, Bonciani F, Callegari I (2013) Photogrammetry and laser scanning for analyzing slope stability and rock fall runout along the Domodossola–Iselle railway, the Italian Alps. Geomorphology 185:110–122. https://doi.org/10.1016/j.geomorph.2012.12.020

Shi GH (1988) Discontinuous deformation analysis – a new numerical model for the statics and dynamics of block system. Ph.D. thesis. Dept. of Civil Engineering, University of California, Berkeley

Shi GH (2001) Three dimensional discontinuous deformation analysis. Proceedings of Fourth International Conference on Analysis of Discontinuous Deformation, pp 1–21

Shi GH (2009) Applications of discontinuous deformation analysis (DDA) to rock engineering. In: Berlin, Heidelberg.Computational mechanics. Springer, Berlin Heidelberg, pp 136–147

Shi GH, Goodman RE (1984) Discontinuous deformation analysis. Proceedings of the 25th US Symposium on Rock Mechanics. pp 269–277
Shi GH, Goodman RE (1989) Generalization of two-dimensional discontinuous deformation analysis for forward modelling. Int J Numer Anal Methods Geomech 13:359–380. https://doi.org/10.1002/nag.1610130403
Spreafico MC, Francioni M, Cervi F, Stead D, Bitelli G, Ghirotti M, Girelli VA, Lucente CC, Tini MA, Borgatti L (2016) Back analysis of the 2014 San Leo landslide using combined terrestrial laser scanning and 3D distinct element modelling. Rock Mech Rock Eng 49:2235–2251. https://doi.org/10.1007/s00603-015-0763-5
Stead D, Wolter A (2015) A critical review of rock slope failure mechanisms: the importance of structural geology. J Struct Geol 74:1–23. https://doi.org/10.1016/j.jsg.2015.02.002
Sturzenegger M, Stead D (2009a) Close-range terrestrial digital photogrammetry and terrestrial laser scanning for discontinuity characterization on rock cuts. Eng Geol 106:163–182. https://doi.org/10.1016/j.enggeo.2009.03.004
Sturzenegger M, Stead D (2009b) Quantifying discontinuity orientation and persistence on high mountain rock slopes and large landslides using terrestrial remote sensing techniques. Nat Hazards Earth Syst Sci 9:267–287. https://doi.org/10.5194/nhess-9-267-2009
Take WA, Chappel M, Brachman R.W.I., Ronald KR (2007) Quantifying geomembrane wrinkles using aerial photography and digital image processing. vol 14. https://doi.org/10.1680/gein.2007.14.4.219
Wang W, Chen GQ, Zhang H, Zhou SH, Liu SG, Wu YQ, Fan FS (2016) Analysis of landslide-generated impulsive waves using a coupled DDA-SPH method. Eng Anal Bound Elem 64:267–277. https://doi.org/10.1016/j.enganabound.2015.12.014
Westin A (2017) Downie slide: an integrated remote sensing approach to characterization of a very slow moving landslide
Wolter A, Stead D, Ward BC, Clague JJ, Ghirotti M (2016) Engineering geomorphological characterisation of the Vajont slide, Italy, and a new interpretation of the chronology and evolution of the landslide. Landslides 13:1067–1081. https://doi.org/10.1007/s10346-015-0668-0
Wu JH (2010a) Compatible algorithm for integrations on a block domain of any shape for three-dimensional discontinuous deformation analysis. Comput Geotech 37:153–163. https://doi.org/10.1016/j.compgeo.2009.08.009
Wu JH (2010b) Seismic landslide simulations in discontinuous deformation analysis. Comput Geotech 37:594–601. https://doi.org/10.1016/j.compgeo.2010.03.007
Wu JH, Chen CH (2011) Application of DDA to simulate characteristics of the Tsaoling landslide. Comput Geotech 38:741–750. https://doi.org/10.1016/j.compgeo.2011.04.003
Wu JY, Li FB (2015) An improved stable XFEM (is-XFEM) with a novel enrichment function for the computational modeling of cohesive cracks. Comput Methods Appl Mech Eng 295:77–107. https://doi.org/10.1016/j.cma.2015.06.018
Wu JH, Lin JS, Chen CS (2009) Dynamic discrete analysis of an earthquake-induced large-scale landslide. Int J Rock Mech Min Sci 46:397–407. https://doi.org/10.1016/j.ijrmms.2008.07.010
Wu W, Zhu H, Lin JS, Zhuang X, Ma G (2018) Tunnel stability assessment by 3D DDA-key block analysis. Tunn Undergr Space Technol 71:210–214. https://doi.org/10.1016/j.tust.2017.07.015
Zhang XP, Wong LNY (2013) Crack initiation, propagation and coalescence in rock-like material containing two flaws: a numerical study based on bonded-particle model approach. Rock Mech Rock Eng 46:1001–1021. https://doi.org/10.1007/s00603-012-0323-1
Zhang Y, Chen G, Zheng L, Li Y, Wu J (2013) Effects of near-fault seismic loadings on run-out of large-scale landslide: a case study. Eng Geol 166:216–236. https://doi.org/10.1016/j.enggeo.2013.08.002

C. Liu · X. Liu (✉) · E. Wang · S. Wang
State Key Laboratory of Hydroscience and Engineering,
Tsinghua University,
Beijing, 100084, China
Email: xiaoli.liu@tsinghua.edu.cn

X. Peng
China Institute of Water Resources and Hydropower Research,
Beijing, 100038, China

S. Wang
Institute of Geology and Geophysics of the Chinese Academy of Sciences,
Beijing, 100029, China